Available online at www.CivileJournal.org

Civil Engineering Journal

(E-ISSN: 2476-3055; ISSN: 2676-6957)

Vol. 11, No. 08, August, 2025

Damage Evolution and Failure Mechanism of Segmental Tunnel Lining

Yang Yu [1, 2], Jinchang Wang [1*], Xinzan Hu [2]

[1] Institute of Transportation Engineering, Zhejiang University, Hangzhou, 310058, China.

[2] Zhejiang Jiangnan Project Management Company Limited, Hangzhou, 310007, China.

Received 07 May 2025; Revised 18 July 2025; Accepted 26 July 2025; Published 01 August 2025

Abstract

The prevention and treatment of damage in segmental tunnel lining structures are critical issues in maintaining tunnel integrity. Understanding the damage evolution and failure mechanisms of these structures is essential for their effective management. This study establishes refined numerical models for shield tunnel segmental linings, incorporating critical factors such as localized weakening around hand holes, multi-interface contact behavior, and embedded reinforcement. A total strain crack model is employed to accurately simulate the nonlinear behavior of concrete. The analysis focuses on the compression-bending failure behavior of segmental joints under positive bending moments and investigates the failure mechanisms of segmental linings subjected to surcharge loading. The results show that the deformation of segmental joints under bending moments can be divided into three stages: linear elasticity, elastoplasticity, and failure. The failure mechanism involves the progressive expansion and penetration of cracks in the core pressure-bearing area, leading to increased crack width, yielding of bolts and rebars, and eventual failure. The overall instability failure of segmental tunnel linings is caused by local failures in areas of low stiffness (joints, hand holes), exhibiting progressive failure characteristics. This study presents significant originality and practical value. A refined analytical model of shield tunnel structures is developed to capture the millimeter-scale cracking characteristics of segmental concrete linings. The model enables precise analysis of the mechanical response of shield tunnels under external construction-induced loading.

Keywords: Shield Tunnel; Segmental Joint; Total Strain Crack Model; Crack Width; Compression-Bending Failure.

1. Introduction

As a critical component of urban rail transit systems, subway tunnels play an essential role in alleviating traffic congestion and have been widely implemented in metropolitan regions around the world. The structural system of shield tunnels typically comprises circular segmental linings connected by bolts, forming a multi-hinged, discontinuous circular arch. This configuration provides the tunnel with a degree of structural flexibility in both longitudinal and transverse directions, enabling it to bear external loads and accommodate deformation in coordination with surrounding soil movements. Construction activities—such as foundation pit excavation—are often inevitable in the vicinity of existing subway lines. These activities frequently result in soil surcharge directly above shield tunnels due to the accumulation of excavated materials [1]. Such sudden and widespread loading can significantly alter the stress distribution within the surrounding soil mass [2]. Under critical conditions, these stress changes may lead to segmental lining deformation [3], structural damage [4], and water ingress [5], ultimately degrading tunnel performance and posing serious risks to operational safety [6, 7]. If existing defects in tunnel linings are not promptly addressed through appropriate reinforcement measures, they may escalate into deep-seated structural damage and eventually cause global

* Corresponding author: wjc501@zju.edu.cn

http://dx.doi.org/10.28991/CEJ-2025-011-08-03

© 2025 by the authors. Licensee C.E.J, Tehran, Iran. This article is an open access article distributed under the terms and conditions of the Creative Commons Attribution (CC-BY) license (http://creativecommons.org/licenses/by/4.0/).

instability of the tunnel system, posing substantial threats to public safety and property. Therefore, in-depth investigation into the damage and deterioration mechanisms of shield tunnels under external loading is of great scientific and engineering significance, as it contributes to improving structural resilience and mitigating the risk of catastrophic failure.

Currently, the mechanical response of shield tunnel segments is primarily studied through four methodological approaches: theoretical analysis, numerical simulation, field monitoring, and physical modeling. Theoretical analyses offer clear mechanical insights and computational simplicity, and have yielded valuable findings in areas such as tunnel settlement, deformation [8], joint dislocation, and joint opening behavior [9]. However, due to their inherent assumptions, these methods are limited in their ability to accurately capture the complex stress distribution within the heterogeneous and discontinuous segmental structure. Field monitoring enables real-time observation of tunnel deformation [10], but lacks the ability to reveal the crack initiation and propagation process under abrupt loading conditions. Laboratory testing provides direct insights into the mechanical behavior and failure modes of tunnel linings [11, 12], however, such tests are costly, time-consuming, and often lack scalability and repeatability. These limitations make them impractical for conducting large-scale parametric studies or for tunnel structural responses.

In contrast, numerical simulation has emerged as a powerful and versatile tool in tunnel engineering research. Its ability to incorporate diverse loading conditions, complex material behaviors, and intricate geometric configurations-along with its efficiency in conducting iterative analyses-makes it indispensable for exploring the structural performance and failure mechanisms of shield tunnels subjected to external loads. Shield tunnels are typically composed of circular precast segments assembled with bolts, where the longitudinal joints represent the most vulnerable components. Under surcharge loading, damage to the segmental lining often initiates at these joints [13]. Therefore, a thorough understanding of the compression-bending failure characteristics and bearing capacity of segmental joints is essential for elucidating the damage evolution and failure mechanisms of shield tunnel linings. Zhang et al. [14, 15] conducted experimental studies on segmental joints under both positive and negative bending moments, focusing on the progression of damage, bolt force development, and joint deformation, as well as assessing the influence of bolts on joint load-bearing capacity. In a subsequent study, Cao et al. [16] conducted a local prototype test on the shear resistance of circumferential joints with tenon connections, examining surface stress distributions, bolt stress responses, and joint openings under various longitudinal forces. While the failure mechanisms at joints have been relatively well explored, the global failure behavior of the entire tunnel lining system remains more complex and less understood.

Zheng et al. [17] established a numerical model of shield tunnel joints using the Coupled Eulerian–Lagrangian (CEL) method to simulate the failure process, elucidate failure mechanisms, and propose three mitigation strategies against progressive failure—subsequently evaluating their effectiveness. Liu et al. [18] performed a full-scale prototype test of shield tunnel joints with staggered segment assembly, analyzing structural deformation, joint opening behavior, and crack propagation patterns to identify failure modes. Zhang et al. [19] employed a concrete plastic damage model to analyze the mechanical behavior of circumferential joints in large-diameter shield tunnels, offering valuable insights into damage evolution and proposing safety evaluation criteria. Shi et al. [20] proposed a bi-scalar damage model to analyze mechanical deformation and failure patterns of shield tunnels under ultimate loading conditions. Zhang et al. [21] conducted a 1:5 scale model test to investigate the stress distribution and deformation characteristics of segmental linings, providing a theoretical basis for structural reinforcement strategies. Ruan et al. [22] developed a three-dimensional numerical model of a shield tunnel that explicitly considers segmental joints, enabling a detailed analysis of stress distribution and deformation characteristics under surcharge loading. Zhu et al. [23] integrated resilience theory into the performance evaluation of shield tunnel structures, constructing a numerical model of segmental lining incorporating historical maximum deformation indices to analyze structural damage behavior. Xie et al. [24] employed a total strain crack model to investigate crack propagation in segmental linings under surcharge conditions and assess the service performance of the structure.

Cracks are among the most common and detrimental defects in shield tunnel segmental linings, significantly compromising the structural serviceability. Crack width serves as a critical design parameter, directly influencing reinforcement strategies and informing tunnel operation and maintenance practices. The development of cracks in segmental linings is typically a progressive process, initiating from localized microcracks and interfacial debonding, and eventually evolving into macro-scale structural damage. To accurately capture this damage evolution, high-resolution simulations at the meso-scale (millimeter level) are indispensable. Consequently, the establishment of a refined numerical model capable of realistically simulating crack initiation, propagation, and failure in shield tunnel linings holds substantial theoretical and practical significance. In recent years, several studies have focused on the damage mechanisms of shield tunnel linings. Wang et al. [25] developed a multi-scale analytical model to simulate the evolution of cracks under loading conditions, offering valuable insights into the underlying fracture mechanisms. Yu et al. [26] proposed a macro–meso multi-scale seismic response model to analyze the longitudinal seismic performance of shield tunnels, which has been successfully applied in engineering practice. Liu et al. [27] constructed a multi-scale numerical model of shield tunnels and surrounding soil based on a double-scalar damage constitutive model for concrete, thereby exploring the degradation behavior of tunnel structures under unloading scenarios.

These studies underscore that the selection of an appropriate concrete constitutive model is crucial for developing refined damage prediction models for shield tunnel linings. Among the available options, the concrete plastic damage model, integrating damage mechanics with classical elastoplasticity-offers a robust constitutive framework. However, its dependence on tensorial variables often leads to increased computational complexity and diminished interpretability of physical behavior. By contrast, smeared crack models offer a more intuitive approach to simulating crack surface behavior and are particularly effective in predicting crack width-a key indicator for structural serviceability. Among them, the total strain crack model has demonstrated excellent performance in capturing structural responses under various loading conditions, including tension/compression, pure bending, and shear. It has also proven effective in simulating coupled loading scenarios such as biaxial shear and tension/compression-bending interactions [28], as well as complex multiaxial stress states. Owing to its predictive accuracy and theoretical robustness, the total strain crack model is recommended by the International Federation for Structural Concrete (fib Model Code 2010) [29] as a standard constitutive model for simulating cracked concrete behavior. Despite its proven effectiveness in general structural applications, the total strain crack model has seen limited implementation in the context of shield tunnel linings. Its potential for modeling the crack evolution and failure mechanisms in such complex underground structures remains underexplored and merits further in-depth investigation.

This study establishes refined numerical models that incorporate detailed representations of longitudinal joints and soil–structure interaction, while employing a total strain crack model to accurately capture the nonlinear and millimeter-scale cracking behavior of concrete, aiming to investigate the progressive damage and failure mechanisms of shield tunnel segmental linings under surcharge loading. The results provide a robust theoretical foundation for ensuring the safe operation and effective maintenance of shield tunnels.

2. Engineering Situation

The study area is located in eastern China, within a metropolitan subway tunnel in the Yangtze River Delta region. Throughout its operational life, the shield tunnel has exhibited multiple forms of structural deterioration, including joint openings, segment cracking, and localized water ingress. Monitoring data identified a significant surcharge zone directly above a specific section of the tunnel alignment, with an affected area of approximately 1600 m². The tunnel is buried at a depth of 7.5 meters within a stratum classified as sandy silt (stratum ③). The general engineering context of the tunnel is illustrated in Figure 1, while the precise geographical location of the study area is presented in Figure 2.

(a) Soil surcharge above the shield tunnel (b) Cracks on the tunnel vault

Figure 1. The tunnel engineering case and information

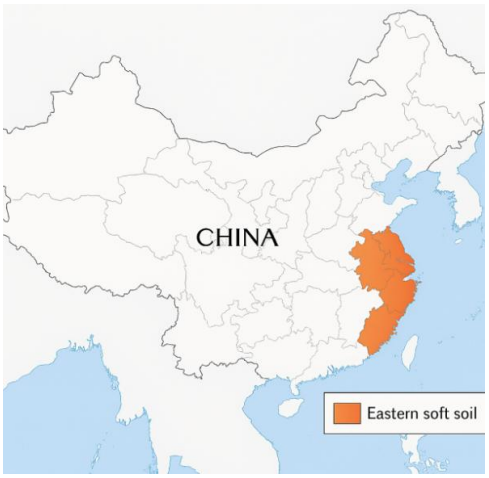

Figure 2. The exact location of the study area

The segmental lining has an outer diameter of 6.2 meters, an inner diameter of 5.5 meters, a thickness of 0.35 meters, and a ring width of 1.2 meters. The configuration of the segmental lining blocks is illustrated in Figure 3. Each joint is reinforced with twelve circumferential bolts of M30 size and 5.8-grade strength, in addition to ten longitudinal M30 bending bolts to ensure structural integrity and load transfer between segments.

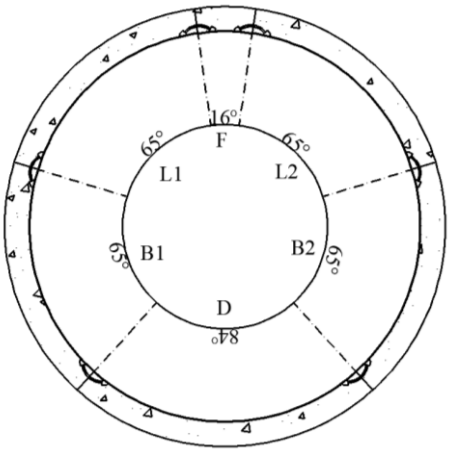

Figure 3. Segmental tunnel lining

3. Compression-Bending Failure Analysis of Segmental Longitudinal Joints

3.1. Numerical Model

This study focuses on the numerical modeling of 1/3-scale segmental longitudinal joints commonly found in standard engineering blocks. Each joint is secured by two longitudinal bending bolts, while embedded bar elements are employed to simulate the internal reinforcement and hand-hole strengthening within the segmental lining, effectively mitigating localized stress concentrations. The primary reinforcement consists of rebar with diameters of 22 mm for the inner layer and 16 mm for the outer layer, supplemented by 10 mm diameter stirrups embedded throughout the segmental lining. Both the bolts and the concrete lining are modeled using three-dimensional solid elements to capture their structural response with high fidelity. The interaction between the bolts, segmental lining, and longitudinal joints is governed by a Coulomb interface friction model, which accurately simulates the slip and rotational behavior at the joint interfaces. This frictional contact behavior is formulated based on generalized strain u and stress vectors t as expressed in the following constitutive relationship:

$$t = \{t_n, t_s, t_t\}^T \tag{1}$$

$$u = \{u_n, u_s, u_t\}^T \tag{2}$$

where t_s and t_t are the shear forces acting on the interface plane, u_s and u_t are the relative shear displacement on the interface plane, t_n and u_n are the traction force and relative displacement perpendicular to the interface plane, respectively. In the elastic state, the expression is :

$$t = D^e u \tag{3}$$

$$D^e = \mathrm{diag}[k_n \quad k_s \quad k_t] \tag{4}$$

where D^e is the elastic stiffness matrix, k_n is normal stiffness coefficient.k_s,k_t are shear stiffness coefficients.

The effective shear stress of friction slip is controlled by the yield function f, and the expression is:

$$f = |\tau| + t_n \tan\varphi - c = 0 \tag{5}$$

$$\tau = \sqrt{t_s^2 + t_t^2} \tag{6}$$

where $\tau$is the effective shear stress, c is the cohesion, φ is the friction angle.

When the friction slip occurs at the interface, the shear traction behavior criterion is :

$$\overline{t_s} = \frac{\overline{\tau}}{\tau} t_s \tag{7}$$

$$\overline{t_t} = \frac{\overline{\tau}}{\tau} t_t \tag{8}$$

where $\bar{t}_s$, $\bar{t}_t$ are the adjusted shear tractions after slip, $\bar{t}$ is limiting shear traction.

The tangential stiffness and normal stiffness of the joint in the model are 5×10^{11} N/m^3 and 8×10^{8} N/m^3, respectively [24]. The segmental lining is connected by solid bolts, the interface opening behavior is set to only compression without tension, the cohesion is 0 MPa, the friction angle is 30°, and the open stress is 0 N/m^2 [24].

Simplifying the complex joint to enhance computational convergence, findings from Zhang et al. [19] indicate that rubber has minimal impact on the bearing performance when stress levels within the segmental lining are high. The numerical model is shown in Figure 4.

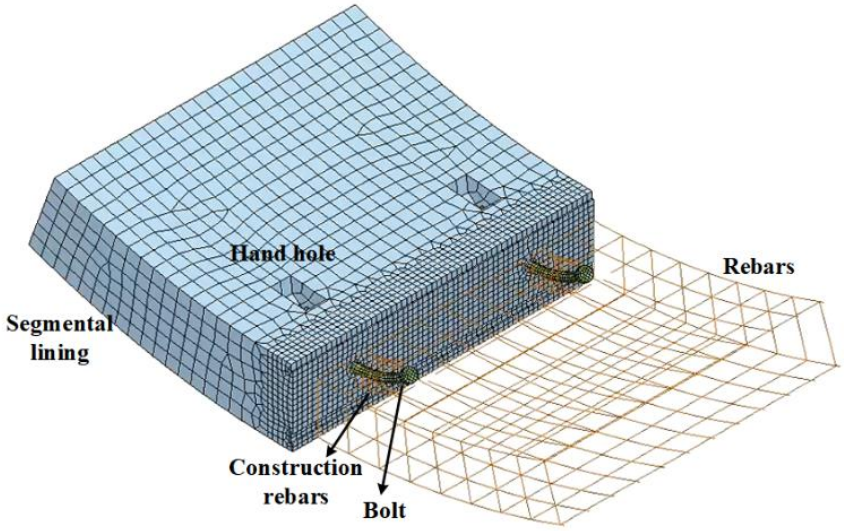

Figure 4. Numerical model of segmental longitudinal joint

3.2. Constitutive Model

The segmental lining is modeled using the total strain crack approach, which primarily characterizes stress development as a function of strain. This method enables precise simulation of the mechanical properties evolution of concrete under tensile, compressive, and shear loads. The core concept of the model involves the combined consideration of crack strain ε_{cr} and elastic strain ε_e. In addition, the magnitude of stress is determined based on the orientation of the crack. The strain vector ε_{xyz} of an element in the *xyz* coordinate system can be expressed as follows:

$$ {}^{t+\Delta t}_{i+1}\varepsilon_{\mathrm{xyz}} = {}^{t}\varepsilon_{\mathrm{xyz}} + {}^{t+\Delta t}_{i+1}\Delta\varepsilon_{\mathrm{xyz}} \tag{9} $$

Using the strain transformation matrix $\boldsymbol{T}$, the strain vector ε_{xyz} is derived through calculated as follows:

$$ {}^{t+\Delta t}_{i+1}\varepsilon_{\mathrm{nst}} = T {}^{t+\Delta t}_{i+1}\varepsilon_{\mathrm{xyz}} \tag{10} $$

The transformation matrix $\boldsymbol{T}$ is determined by the principal stress direction within the element. Its formulation is given by:

$$ T = T({}^{t+\Delta t}_{i+1}\varepsilon_{\mathrm{xyz}}) \tag{11} $$

Conversely, the stress vector is first computed within the crack-local coordinate system ${}^{t+\Delta t}_{i+1}\sigma_{\mathrm{nst}}$:

$$ {}^{t+\Delta t}_{i+1}\sigma_{\mathrm{nst}} = f({}^{t+\Delta t}_{i+1}\varepsilon_{\mathrm{nst}}, \theta) \tag{12} $$

where θ represents the angle threshold that differentiates various crack orientations.

The corresponding stress vector is expressed as:

$$ {}^{t+\Delta t}_{i+1}\sigma_{\mathrm{xyz}} = T^{T} {}^{t+\Delta t}_{i+1}\sigma_{\mathrm{nst}} \tag{13} $$

For nonlinear segment analysis, particularly in evaluating the ultimate load-bearing capacity of an individual segment, prior studies have validated the accuracy of the smeared crack constitutive model through experimental and

numerical investigations [30]. The crack orientation parameter (denoted as angle q) in the total strain crack model was determined based on existing literature and widely accepted modeling practices. Specifically, we adopted a value of q = 45°, which reflects the typical orientation of cracks under combined tension-compression and shear conditions in concrete structures, as validated by previous studies. This assumption aligns with the recommendations of the fib Model Code [29] and has been shown to yield reliable predictions in similar structural configurations. Nonetheless, we acknowledge that crack orientation can be influenced by material heterogeneity, loading direction, and boundary conditions. The material parameters are detailed in Table 1.

Table 1. Material parameters

Material	Type	Young's modulus (MPa)	Poisson's ratio	Tensile stress (MPa)	Compressive stress (MPa)	Tensile fracture energy (N/m)
Segmental lining	C50	3.45×10^4	0.2	1.89	23.1	151
Rebar	HRB335	2×10^5	0.3	335	—	—
Joint bolts	M30	2.1×10^5	0.2	400	—	—

The rebar and bolts are modeled using the Von-Mises plastic hardening constitutive model. Rebar behavior is simulated using embedded bar elements, with a protective concrete layer thickness of 50 mm.

3.3. Loading Method

The numerical analysis reveals that under surcharge conditions, the maximum axial force acting on the segmental lining and joint reaches 1800 kN, corresponding to an axial compression ratio of 0.2. The relationship between joint internal forces and external loading was established using the internal force model for segmental joints as proposed in Liu et al. [18]. During the entire loading process, the horizontal load remains constant, while incremental increases in vertical load result in a progressive rise in the bending moment acting on the joint. Once a critical threshold is exceeded, significant structural damage is observed. Table 2 summarizes the applied horizontal load values along with their associated maximum vertical loads, offering quantitative insight into the joint's load-bearing capacity under combined loading scenarios.

Table 2. Loading conditions of experiments

Loading method	Horizontal load (kN)	Maximum vertical load (kN)
Positive moments	1800	787.5

The experimental loading conditions are illustrated in Figure 5. The loading protocol is implemented in two stages: first, a uniform horizontal load is applied to both lateral supports of the segmental lining to induce axial compression. Once the axial force reaches a target value of 1800 kN, it is maintained constant. Subsequently, a vertical load is incrementally applied from zero to its maximum value to progressively increase the bending moment acting on the structure. This staged loading continues until structural instability and ultimate failure are observed. The overall methodology and numerical workflow are outlined in the flowchart presented in Figure 6.

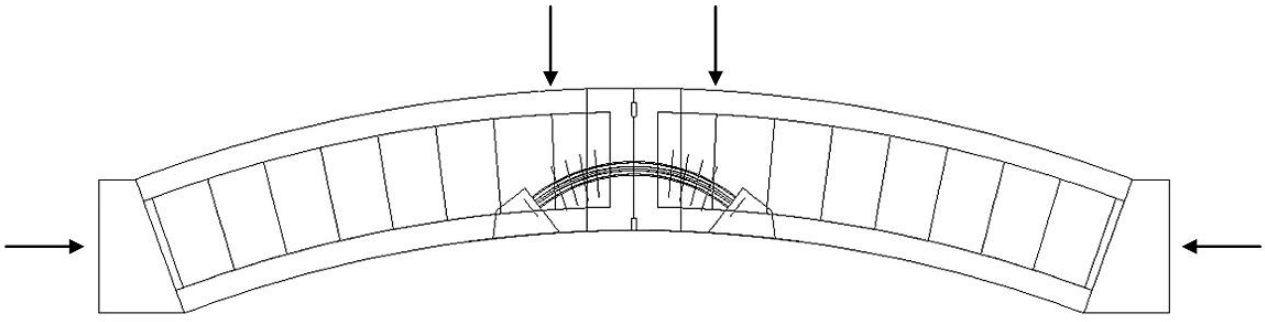

Figure 5. Positive moments in the numerical models

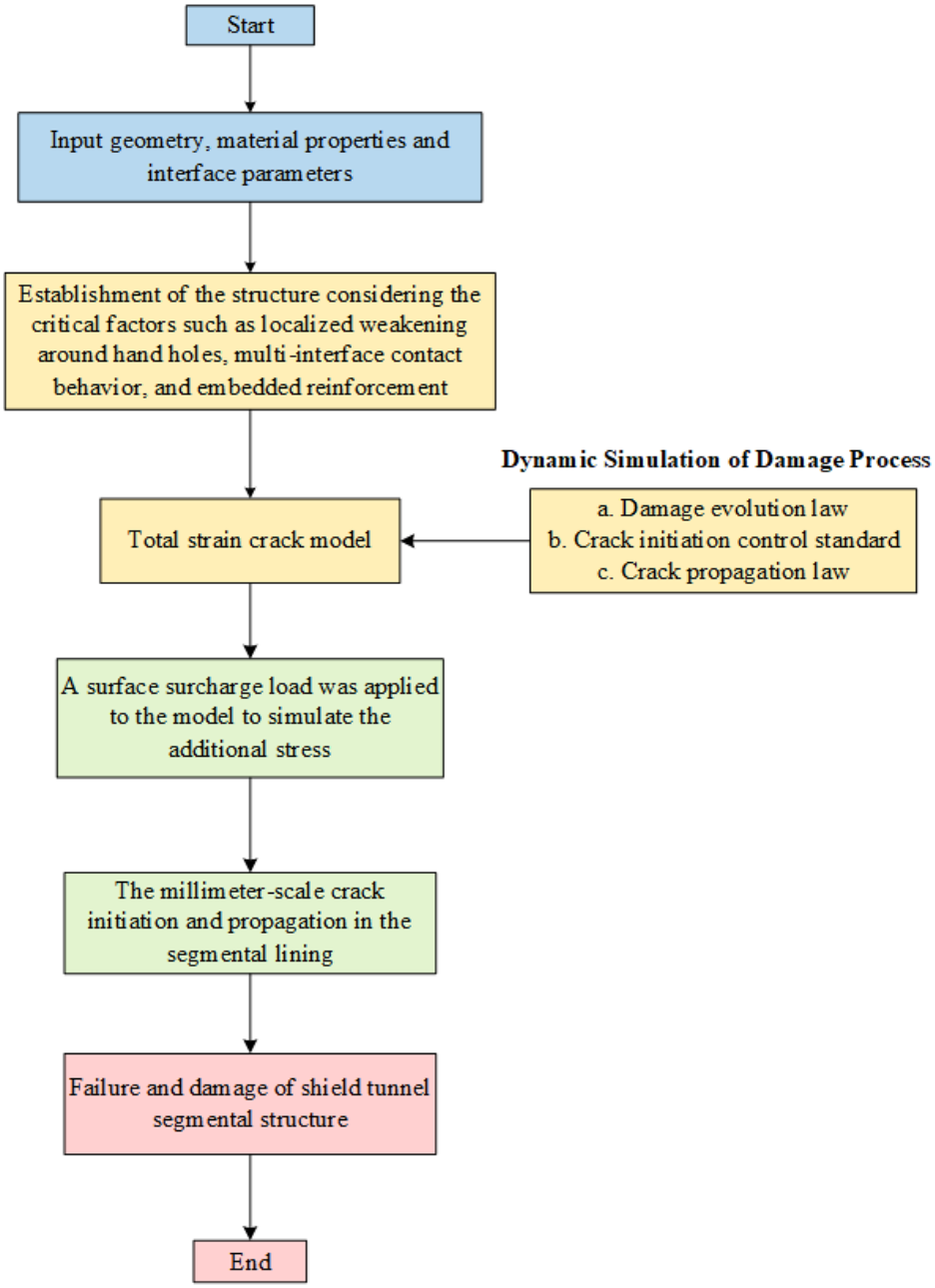

Figure 6. Flowchart presenting the workflow and methodology

3.4. Analysis of the Result

3.4.1. Calculation Verification

Based on the aforementioned constitutive model and numerical approach, simulations were performed and validated against the experimental results of compression-bending failure tests on segmental joints reported in Zhang et al. [14]. The internal force–bending moment relationship is illustrated in Figure 7, and the corresponding failure mode of the segmental joint is shown in Figure 8. The numerical results accurately capture the moment–displacement trend observed in the experiment, including the nonlinear stiffness degradation and crack evolution stages. Quantitatively, the peak bending moment from the experiment reaches approximately 450 kN·m, while the numerical simulation predicts a peak of 410 kN·m, resulting in a deviation of approximately 8.9%. The vertical displacement at which peak bending occurs is also closely matched, with the simulation capturing the transition from elastic to inelastic behavior. Notably, the predicted crack initiation and propagation paths-starting from the bolt interfaces and extending along the concrete surfaces-closely mirror the experimental observations. This strong agreement in both load–displacement behavior and failure morphology underscores the effectiveness of the total strain crack model in reproducing the millimeter-scale cracking behavior typical of segmental joints under compression–bending interaction. These findings validate the model's reliability and establish its suitability for advanced structural performance assessments in shield tunnel engineering.

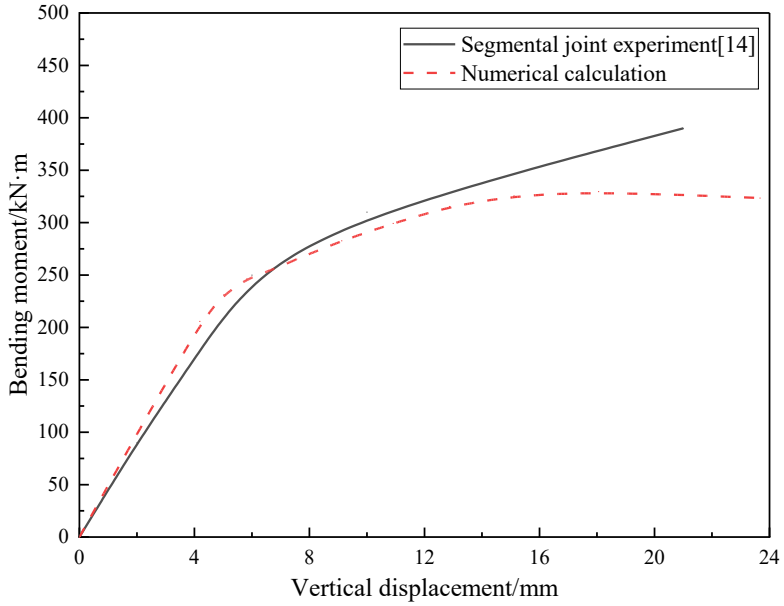

Figure 7. Segmental longitudinal joint model verification curve

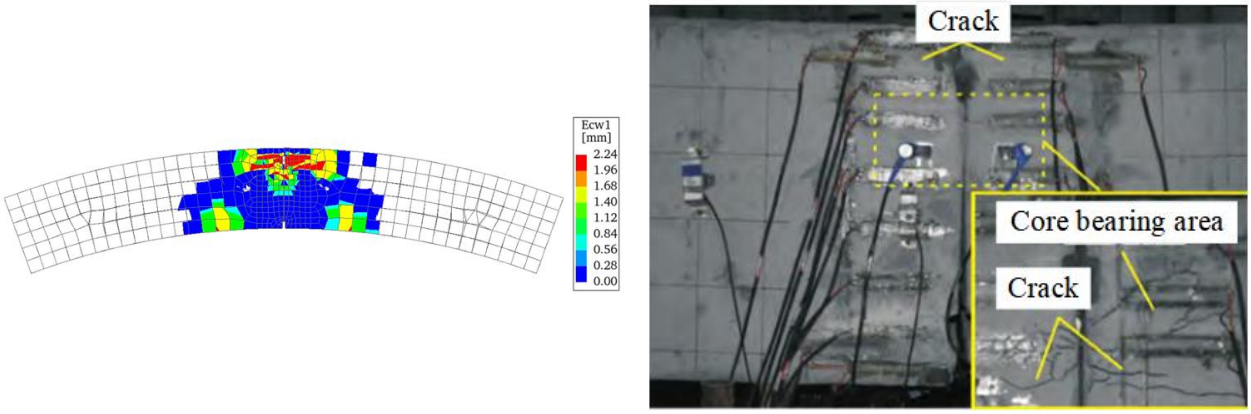

(a) Numerical calculation (b) Segmental joint experiment [14]

Figure 8. Comparison between numerical simulation results and experimental failure behavior

Although the primary focus of this study is the validation of numerical results against representative experimental data, it is important to acknowledge potential uncertainties inherent in physical testing. Among these, variability in concrete compressive strength may significantly influence structural performance. In the present model, a compressive strength of 23.1 MPa was adopted, corresponding to the mean value reported in the referenced experiments [14]. Preliminary sensitivity analyses indicated that even small deviations (±5–10%) in this parameter could lead to noticeable differences in the predicted peak moment and crack initiation timing. While a full probabilistic analysis is beyond the current study's scope, these findings highlight the importance of material variability. Future work will consider incorporating stochastic methods to more rigorously quantify the effects of such uncertainties on model reliability.

Compared to previous numerical studies that utilized simplified contact definitions or elastic-plastic constitutive assumptions, the present model introduces refined representations of reinforcement, localized weakening near hand holes, and multi-interface contact behavior, leading to enhanced fidelity in simulating real-world tunnel behavior. Furthermore, while prior experimental works such as those by Zhang et al. [14, 15] focused primarily on load–displacement response and bolt forces, the present study extends the analysis by revealing the spatial-temporal evolution of cracks and stress redistribution in a more granular manner. Overall, the comparison underscores the validity of the refined numerical approach and highlights its advantages in delivering comprehensive insights into the failure mechanisms of shield tunnel segmental joints under complex loading conditions.

3.4.2. Stress and Deformation Behavior of Segmental Joints

The deformation and stress characteristics of segmental longitudinal joints under positive bending moments are illustrated in Figure 9. As shown in Figure 9-a, both the bending moment and vertical displacement exhibit pronounced nonlinear behavior with increasing load. Based on the evolution of joint opening and bolt stress distribution, the

deformation process of the segmental joint can be categorized into three distinct stages. Stage I - Linear Elastic Phase: The bending moment increases linearly with vertical displacement, while the joint maintains relatively stable deformation. During this stage, the moment-displacement curve transitions from steep to gradually increasing, and the rotation angle begins to rise. The joint's load-bearing capacity is primarily sustained by the bolts (Figure 9-b). No visible cracks are observed, and the joint remains structurally intact. Stage II - Elastic-Plastic Phase: In this stage, the rate of increase in bending moment slows, while vertical displacement accelerates. At the end of this phase, the vertical displacement reaches 5.3 mm, and the bending moment attains 250.8 kN • m. The joint opening becomes substantial, and the bolts begin to yield under combined bending and axial tension. The stress concentrates near the bolt-concrete interface, with tensile stress in the bolts reaching 400 MPa (Figure 9-c), entering the plastic range. Stage III - Failure Phase: This phase is characterized by diminishing structural stiffness and increasing deformation. The maximum vertical displacement reaches 13.93 mm (Figure 9-d), and the joint opening extends to 1.38 mm (Figure 9-e). Tensile stress in adjacent longitudinal rebars rises to 335 MPa (Figure 9-f), indicating localized yielding. As the structural capacity deteriorates, cracks initiate and propagate through the joint section. Once these cracks coalesce and extend across the segmental interface, complete joint failure ensues, leading to a loss of bearing capacity

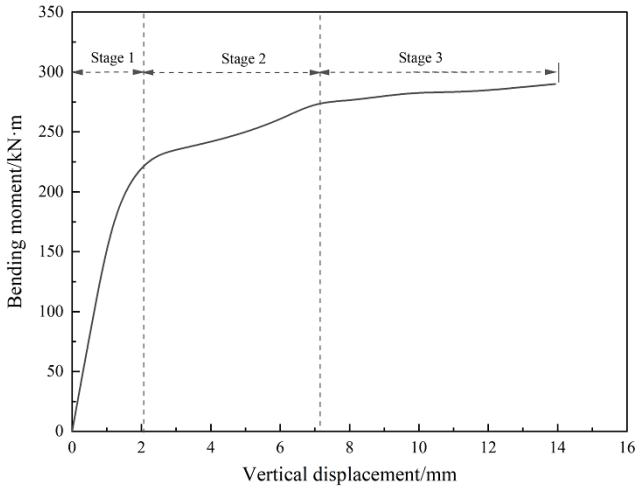

(a) Bending moment-vertical displacement of segmental joint

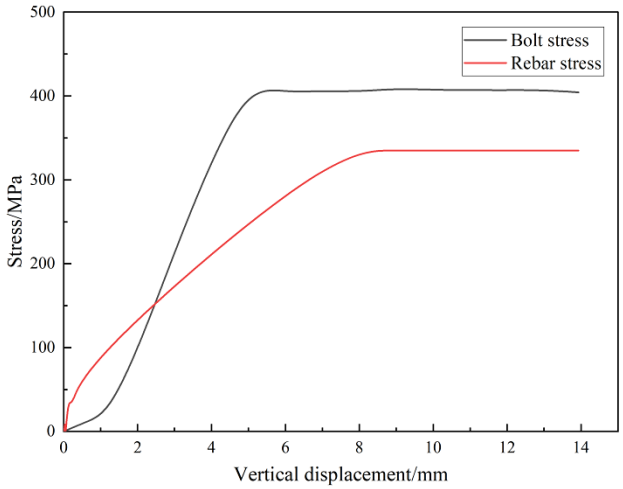

(b) Bolt and rebar stress-vertical displacement

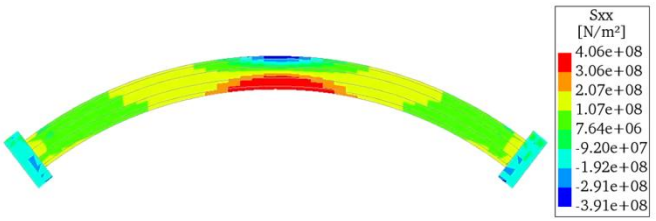

(c) Bolt stress

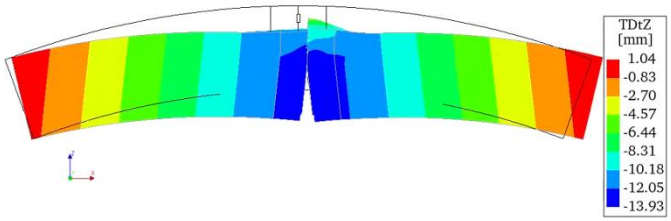

(d)Vertical displacement of segmental joint

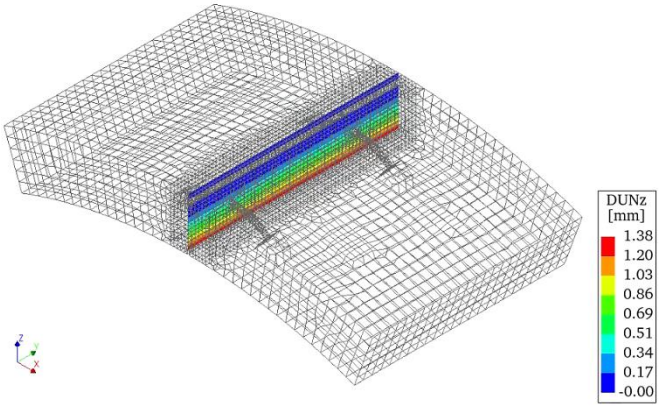

(e) Opening of segmental joint

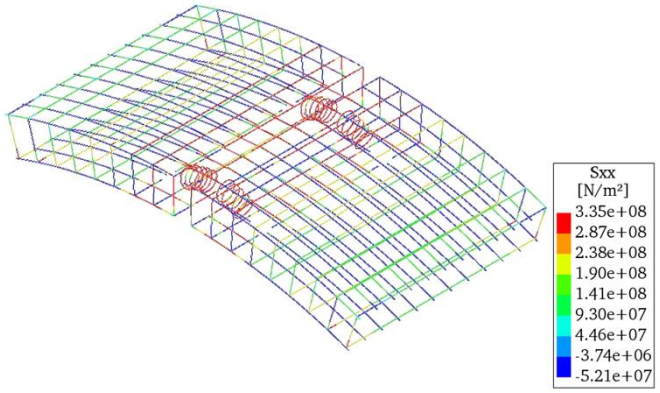

(f)Rebar stress

Figure 9. Deformation and stress characteristics of segmental longitudinal joints under positive moments

3.4.3. Crack Characteristics of Segmental Joints

Figure 10 illustrates the crack widths and damage factors observed at the ultimate failure of segmental joints subjected to positive moments. The crack distribution under positive moment loading is consistent, predominantly

characterized by longitudinal cracks. The maximum crack width reaches 2.24 mm. Significant damage is concentrated near the core bearing area of the joint, extending outward along both sides of the joint interface. Notably, extensive deterioration occurs around the hand holes and bolt holes, attributed to the combined effects of tension, compression, and shear forces imposed by the bolts and concrete. The damage and failure process can be described as follows: with increasing vertical load, the joint opening progressively enlarges, resulting in a reduction of the concrete contact area within the core bearing region and initiating crack formation that propagates outward. As the extrusion intensifies, crack widths increase until the joint ultimately fails. Cracks predominantly develop on the upper side of the core bearing area, which consistently sustains the vertical loads.

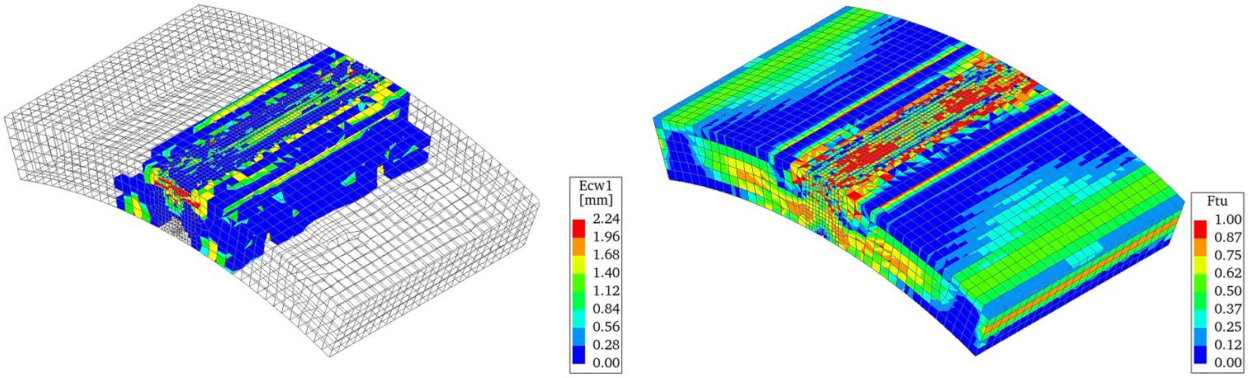

(a) Crack width (b) Damage factor

Figure 10. Crack width and damage factor of segmental longitudinal joints

Based on the analysis of internal forces, stress distribution, vertical deformation, and joint openings depicted in Figures 9 and 10, the failure mechanism of the segmental joint is governed by crack initiation and propagation within the core pressure-bearing zone. Initially, crack widths increase gradually as the load escalates, leading to yielding of bolts and reinforcement bars. With further crack propagation and widening, the structural stiffness deteriorates progressively, culminating in the failure of the segmental joint and a consequent loss of its load-bearing capacity.

4. Failure Mechanism of Segmental Lining

4.1. Soil-Structure Analysis Model

The soil-structure model is developed based on the actual project dimensions, following the procedures and constitutive models described in Section 3.1. Liu et al. [27] concluded that when a shield tunnel reaches its ultimate bearing capacity, the multi-ring assembly effect has minimal influence on the mechanical behavior of the structure; thus, this study focuses on the damage mechanisms of a single-ring shield tunnel. The segmental lining within the soil-structure model accounts for local weakening caused by features such as hand holes, multiple contact points, and reinforcement bars. The interaction between the segmental lining and the surrounding soil is simulated using interface elements governed by Coulomb friction, with tangential and normal stiffness values set at 1×10^{8} N/m^3 and 2×10^{12} N/m^3, respectively [24]. To represent ground surcharge and the excavation influence zone, the soil domain dimensions are set to 75 m in length, 40 m in height, and 1.2 m in width, emphasizing the critical tunnel cross-section. Boundary conditions are imposed as follows: the top surface is free; the bottom boundary is fixed in the vertical (Y) direction; the front and rear faces are constrained along the longitudinal (Z) axis; and the lateral boundaries are restrained in the horizontal (X) direction.

Based on the results reported in Liu et al. [27], the soil properties are summarized in Table 3. The Mohr-Coulomb constitutive model is employed to represent the soil mechanical behavior, incorporating initial in-situ stresses. A lateral earth pressure coefficient of 0.5 is adopted in the simulations.

Table 3. Properties of soil

Soil	Density (kg/m^3)	Poisson's ratio	Young's modulus (MPa)	Cohesion (kPa)	Friction angle (°)	Soil height (m)
②$_1$Sand silty	1880	0.27	25	13.5	31.9	2
③$_2$Sand silty	1900	0.27	25	9.2	30.1	4
③$_5$Sand silty	1860	0.27	25	9.5	27.4	8
③$_6$Muddy silty clay mixed with silty clay	1810	0.3	20	9.8	23.7	10
⑥$_2$Muddy clay	1720	0.3	15	16.9	16.7	16

4.2. Construction Process of the Surcharge

A detailed model of the surcharge geotechnical body was developed using Diana 10.5, as shown in Figure 11. This model systematically captures the interaction between the segmental lining and the surrounding soil. The tunnel structure and geotechnical domain were discretized with differing mesh sizes: segmental lining elements measure 0.06 m, while geotechnical elements are sized at 1 m. The surcharge load was applied following a phased construction sequence outlined in Table 4. In the initial stage, all rock and soil elements were activated to equilibrate the in-situ stresses. During the second stage, soil elements within the tunnel excavation zone were removed to simulate excavation. The third stage involved activation of the segmental lining, bolts, and reinforcement bars. Finally, in the fourth stage, the surcharge was incrementally imposed in four increments with load factors of 0.25, 0.5, 0.75, and 1.0 to simulate surcharge construction. The surcharge load is simplified as a uniform pressure applied at the ground surface, as illustrated in Figure 11. The equivalent uniform load value of 180 kPa was derived based on parameters relevant to the heaped soil [23].

Table 4. Surcharge construction process

Stage	Condition
Step 1	Initial stress balance of soil
Step 2	Tunnel excavation
Step 3	Activation of segmental lining, bolts, and rebars
Step 4	Surcharge application in 4 steps: load factors 0.25, 0.5, 0.75, and 1.0

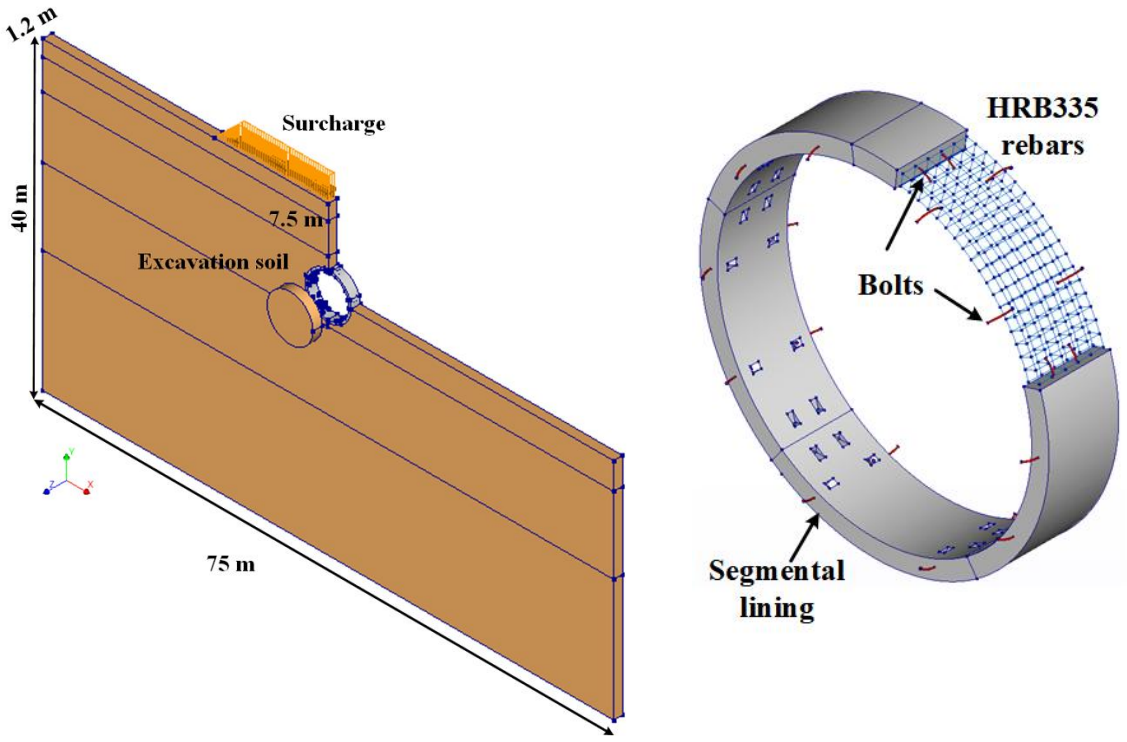

Figure 11. Numerical model of the Soil-Segmental Lining Structure

4.3. Numerical Results

4.3.1. Vertical Deformation of Segmental Lining

Using the constitutive models and modeling approaches described above, the dimensions and material parameters from the model tests reported in He et al. [32] were adopted for the numerical analysis of the shield tunnel structure. The calculation results are presented in Figure 12. As illustrated, the vertical deformation of the soil–shield tunnel model exhibits close agreement with the experimental data from He et al. [32]. The strong correlation between the numerical simulations and physical tests verifies that the constitutive model employed effectively captures the stress distribution within the segmental tunnel lining, thereby confirming its reliability in analyzing the structural mechanical response.

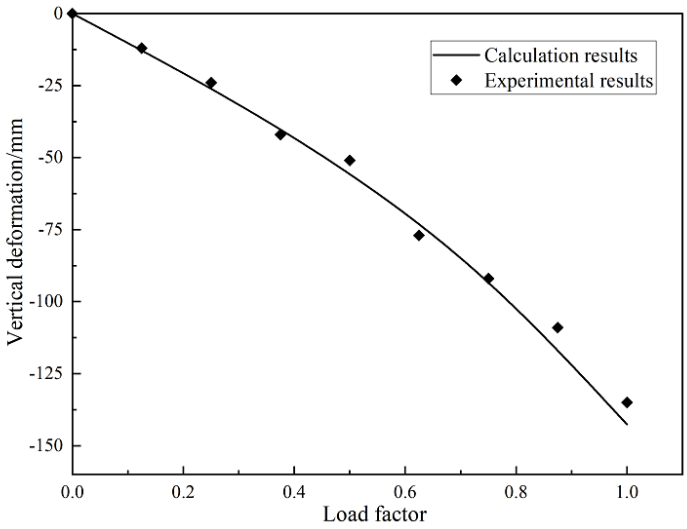

Figure 12. Comparative Analysis of Vertical Deformation in Shield Tunnel Structures

Figure 13 illustrates the vertical deformation behavior of the shield tunnel under surcharge loading, revealing pronounced settlement patterns and an evidently asymmetric displacement distribution along the tunnel cross-section. The analysis shows that the segmental lining undergoes differential deformation, with the arch vault-directly beneath the surcharge influence zone-exhibiting significantly greater vertical displacement compared to the arch bottom. Quantitatively, the maximum settlement at the vault reaches 76.6 mm, which exceeds the deformation at the arch bottom by approximately 15% (vault-to-bottom deformation ratio: 1.15). This uneven deformation pattern suggests a clear influence of surcharge-induced stress redistribution within the surrounding soil mass, leading to an 'elliptical' or vertically compressed tunnel profile. Such asymmetry not only elevates the risk of joint opening and structural cracking at the upper segment interfaces but also amplifies localized stress concentrations, potentially accelerating fatigue damage over the service life of the tunnel.

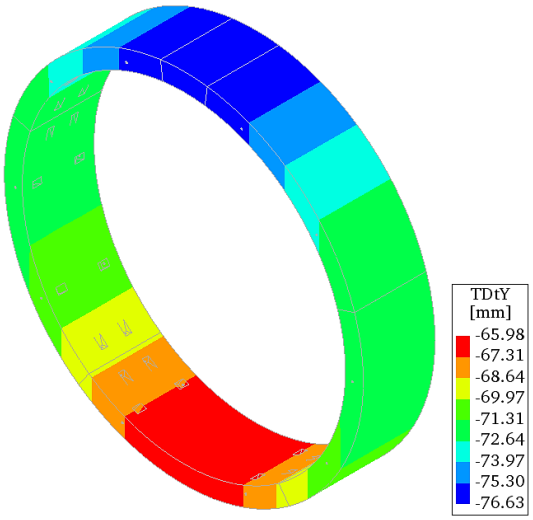

Figure 13. Vertical deformation of the shield tunnel

4.3.2. Segmental Joint Stress and Deformation

The vertical deformation analysis of the shield tunnel indicates that surcharge loading induces notable structural responses, particularly in the form of joint opening between segmental linings. As illustrated in Figure 14, the longitudinal joint openings exhibit a distinct spatial pattern, with the maximum opening of 2.08 mm occurring at the vault joint, which corresponds to the region subjected to the highest positive bending moment. This deformation pattern highlights the mechanical vulnerability of the vault segment under surcharge-induced loading conditions. The overall deformation mode of the tunnel lining resembles an elliptical profile, resulting from non-uniform soil pressure redistribution caused by the surcharge. This deformation induces tensile stresses at the vault and haunch zones, which are typically the most flexible and least restrained parts of the segmental assembly.

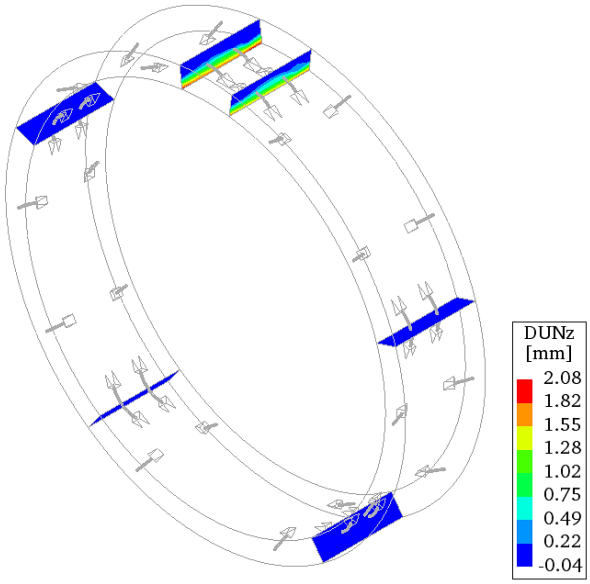

Figure 14. Segmental joint opening of shield tunnel

Consequently, the joints in these regions are more susceptible to separation and cracking, which can compromise the tunnel's watertight integrity and long-term durability. The analysis underscores the critical importance of targeted waterproofing and joint sealing measures, especially at the vault and haunch positions, in real-world engineering applications.

Figure 15 illustrates the tensile stress distribution of the 12 circumferential bolts embedded within the shield tunnel segmental lining under surcharge loading. The results reveal a clear gradient in bolt stress along the cross-section of the lining, closely correlating with the degree of joint opening. Specifically, bolt stress decreases progressively from the arch vault toward the arch bottom, reflecting the distribution of bending moments and segmental separation. The maximum tensile stress, recorded at the vault bolts, reaches approximately 400 MPa, which approaches or exceeds the typical yield strength of standard structural steel bolts. This observation indicates that localized yielding of bolts is likely to occur under extreme surcharge conditions, particularly in the vault region where joint opening is most severe. In contrast, bolts at the arch bottom exhibit the lowest tensile stress, measured at 48 MPa, due to the compressive nature of the stress field in that region, which suppresses joint separation and bolt elongation.These findings underscore the non-uniform mechanical demand placed on circumferential bolts throughout the lining structure, with vault bolts experiencing the most unfavorable loading conditions. Such stress concentrations may accelerate fatigue damage or long-term creep, particularly in shield tunnels operating in soft soil environments with fluctuating surcharge influences. Therefore, additional reinforcement strategies, such as bolt material upgrading or the use of preload-tightening methods, should be considered in high-stress zones to enhance overall structural reliability.

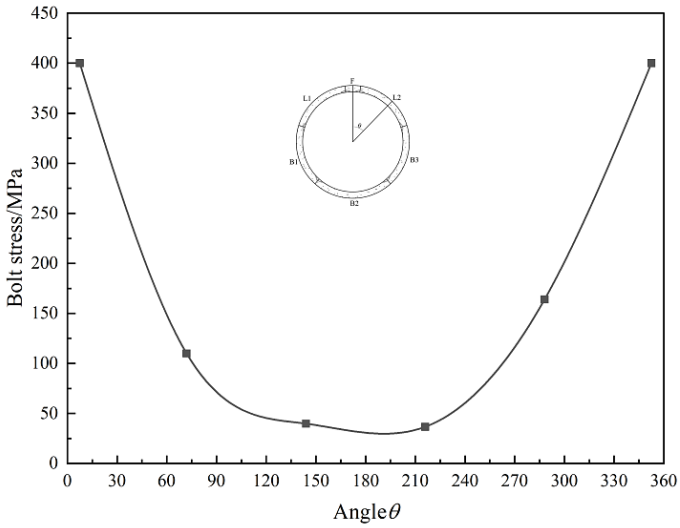

Figure 15. Bolt stress of shield tunnel

Figure 16 illustrates the distribution and evolution of internal forces within the shield tunnel segmental lining under surcharge loading. In this analysis, axial force is defined as positive in compression, while bending moment is considered positive when the outer face of the lining section is subjected to tensile stress. At the initial stage of loading, tensile stresses develop along the inner surfaces of the arch vault and bottom, reflecting the influence of vertical loads transmitted through the surrounding soft soil. Concurrently, the transverse direction of the tunnel exhibits tensile behavior, primarily due to the ovalization effect induced by vertical overburden pressure. Notably, the left haunch exhibits relatively higher axial compressive forces compared to other regions, suggesting that this area experiences more favorable stress states, potentially due to asymmetric boundary conditions or local stiffness variations in the surrounding soil. As the surcharge load increases, the overall stiffness of the longitudinal joints degrades, especially at the vault and haunch regions. This reduction in stiffness leads to localized curvature changes and a redistribution of internal forces, resulting in a concentration of bending moments in structurally vulnerable zones. The axial force evolution mirrors the bending moment trends, with sharp increases observed at the arch vault, arch bottom, and both haunches, highlighting their critical roles in resisting external loads. This behavior indicates that the structure undergoes a transition from an initially uniform stress distribution to a more nonlinear, damage-prone state under intensified surcharge. The simultaneous escalation of both axial and flexural stresses may significantly reduce the safety margin of the lining, particularly in aging tunnels or those with pre-existing defects.

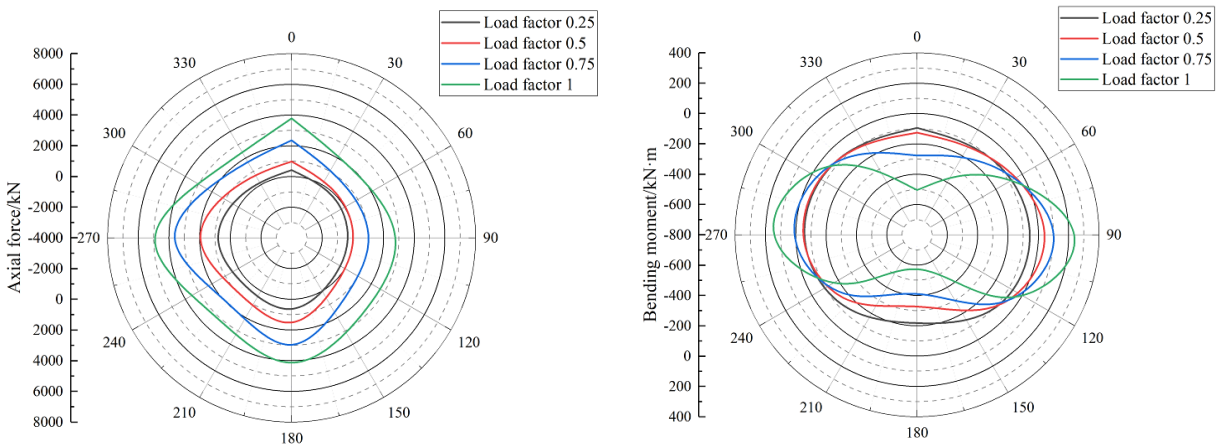

(a) Axial force (b) Bending moment

Figure 16. Internal force of segmental lining

4.3.3. Progressive Failure Process

Figure 17 illustrates the evolution of crack propagation in the segmental lining under progressive surcharge loading. After the initial loading phase, microcracks begin to emerge in regions of stress concentration and structural weakness—primarily along the longitudinal joints and around hand holes located in tensile zones. These early-stage cracks, with a maximum width of 0.22 mm (Figure 17-a), suggest that stress redistribution initiates in areas with reduced stiffness and reinforcement continuity. As the surcharge increases to the second loading step, crack extension becomes more pronounced. The damage spreads from the initially affected zones to the inner surfaces of the arch vault and bottom, as well as the outer edge of the right haunch. The maximum crack width increases to 0.53 mm (Figure 17-b), indicating the progression from localized damage to structural deterioration. Interestingly, the left haunch remains unaffected, likely due to asymmetrical loading or structural heterogeneity leading to an uneven stress field. At the fourth surcharge step, the segmental lining undergoes extensive cracking. Cracks along the longitudinal joints and tensile regions coalesce and propagate deeper, culminating in the formation of map cracking patterns that cover large surface areas. The maximum crack width reaches 2.05 mm (Figure 17-d), signifying a critical loss of structural integrity. The progression from isolated microcracks to widespread macrocracking underscores the nonlinear deterioration behavior of the lining and highlights the critical role of tensile zones in initiating failure. These findings emphasize the importance of enhanced waterproofing, monitoring, and targeted reinforcement in vulnerable regions to ensure long-term tunnel safety under complex ground loading conditions.

The failure process of the segmental lining can be broadly categorized into three stages. The first stage is the initial elastic stage, where the vertical deformation of the segmental lining steadily increases, accompanied by joint opening inside the tunnel, as well as a rise in bolt stress. The second stage is the local failure stage: cracks initiate and expand in areas of lower stiffness, such as joints and hand holes. The width of these cracks progressively increases. The third stage is the overall instability stage: cracks extend through the entire section in the tensile zones and around hand holes. The segmental lining exhibits characteristics of progressive failure leading to overall instability and failure.

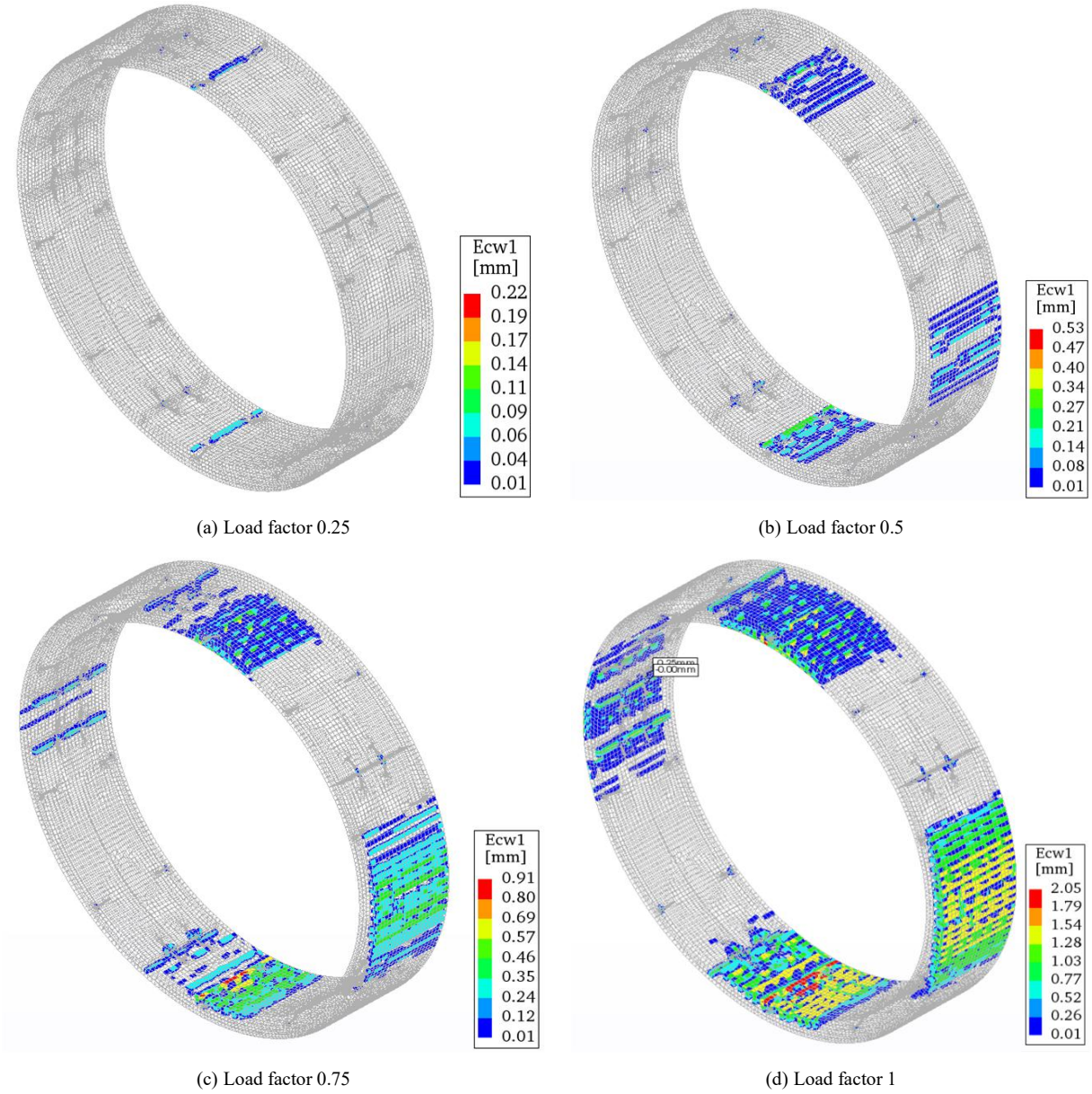

(a) Load factor 0.25

(b) Load factor 0.5

(c) Load factor 0.75

(d) Load factor 1

Figure 17. Crack propagation process of shield tunnel

4.3.4. Discussion of Crack Width and Operational Criteria

The numerical simulations conducted in this study revealed a maximum crack width of 2.05 mm in the segmental lining under surcharge loading conditions. This value significantly exceeds commonly accepted serviceability limits for shield tunnel structures. According to design codes [33], the allowable crack width for water-retaining underground concrete structures is typically restricted to 0.2–0.3 mm to ensure long-term durability, corrosion resistance of embedded reinforcement, and water-tightness. Even in less aggressive environments, a maximum threshold of 0.4 mm is rarely exceeded. The predicted crack widths in this study clearly indicate that the structural integrity and waterproofing performance of the segmental lining would be severely compromised under the evaluated surcharge conditions. This level of damage poses a substantial risk to tunnel serviceability and safety, particularly in water-bearing strata where ingress may cause progressive deterioration of the structure, trigger joint dislocation, or even initiate localized instability. These findings underscore the urgent need for remedial actions when early signs of segmental cracking or joint opening are detected. In practical engineering, suitable reinforcement measures-such as external bonding of steel plates, application of fiber-reinforced polymers (FRPs), joint injection grouting, or circumferential prestressing—should be considered to enhance structural resilience. Additionally, routine inspection and health monitoring systems should be implemented to detect and quantify crack development in high-risk zones such as the tunnel vault and spandrels. This study highlights the importance of integrating crack width prediction into tunnel safety evaluations and provides a robust theoretical basis for defining warning thresholds and formulating intervention strategies under extreme loading conditions.

5. Conclusion

In this study, an enhanced segmental joint model and a coupled soil–structure interaction numerical framework were developed to investigate the compression-bending failure of segmental joints and the progressive failure mechanism of shield tunnels under surcharge conditions. The simulation results based on the total strain crack model demonstrated strong agreement with experimental observations, particularly in capturing the bending characteristics of segmental joints and providing detailed millimeter-scale crack propagation patterns. The failure mechanism of the segmental joints was identified as a progressive process starting with crack initiation in the core bearing zones. As loading increased, the cracks widened, and yielding of bolts and reinforcement bars occurred, leading to further crack penetration and a gradual reduction in joint stiffness. This sequence ultimately culminates in joint failure and a loss of bearing capacity.

Under surcharge loading, the segmental lining exhibits an elliptical deformation pattern, with the arch vault experiencing the greatest vertical displacement. This deformation results in pronounced joint openings at the vault and spandrel regions, where the maximum recorded gap reaches 2.08 mm-highlighting these areas as critical zones of stress concentration. Moreover, the vertical settlement exceeds 76 mm, which substantially surpasses the standard safety thresholds for metro tunnel operation. These findings indicate a high risk of compromised structural integrity and serviceability under such loading conditions. Consequently, targeted reinforcement measures-such as joint sealing, external confinement, or structural retrofitting-are essential to mitigate the potential for further deterioration and ensure long-term tunnel safety. Furthermore, the entire failure evolution of the segmental lining could be divided into three distinct stages: an initial elastic phase, a crack propagation stage concentrated at segmental joints and hand holes, and a final phase characterized by global structural instability. This clearly reflects a progressive failure mode inherent to shield tunnels under external loading. Overall, the findings provide a more accurate depiction of joint behavior and failure evolution, offering theoretical support for the design, evaluation, and reinforcement of shield tunnel linings in complex geotechnical environments.

6. Declarations

6.1. Author Contributions

Conceptualization, Y.Y.; methodology, Y.Y.; software, Y.Y.; validation, Y.Y., J.W., and X.H.; formal analysis, Y.Y.; investigation, Y.Y.; resources, Y.Y.; data curation, Y.Y.; writing—original draft preparation, Y.Y.; writing—review and editing, Y.Y.; visualization, Y.Y.; supervision, Y.Y.; project administration, X.H.; funding acquisition, J.W. All authors have read and agreed to the published version of the manuscript.

6.2. Data Availability Statement

The data presented in this study are available on request from the corresponding author.

6.3. Funding

This study is funded by the Zhejiang Jiaogong Collaborative Innovation Joint Research Center Project (No: ZDJG2021004).

6.4. Conflicts of Interest

The authors declare no conflict of interest.

7. References

[1] La, H., Nguyen-Minh, T., & Nguyen, T. (2025). Optimized prediction of tunnel stability using advanced machine learning and an ANN-based analytical expression. Tunnelling and Underground Space Technology, 164, 106778. doi:10.1016/j.tust.2025.106778.

[2] Nilot, E. A., Fang, G., Li, Y. E., Tan, Y. Z., & Cheng, A. (2023). Real-time tunneling risk forecasting using vibrations from the working TBM. Tunnelling and Underground Space Technology, 139, 105213. doi:10.1016/j.tust.2023.105213.

[3] Feng, D.-L., Wu, H.-N., Meng, F.-Y., Yang, S.-Q., & Chen, R.-P. (2025). Investigation on structural performance of segmental linings of shield tunnels under loading–unloading-reloading condition. Tunnelling and Underground Space Technology, 157, 106331. doi:10.1016/j.tust.2024.106331.

[4] Yu, Y., & Wang, J. (2025). Crack mechanism of shield tunnel under excavation of foundation pit. AIP Advances, 15(2), 0249750. doi:10.1063/5.0249750.

[5] Hu, Z., Zhang, C., Meng, S., Du, Y., Ma, K., Wang, H., Qie, B., & Xu, S. (2025). Encapsulated anti-aging approach on rubber sealing gasket of shield tunnel segment joint: a multiscale comparative experimental study. Tunnelling and Underground Space Technology, 164, 106854. doi:10.1016/j.tust.2025.106854.

[6] Sun, Y., Yu, Y., Wang, J., & Wang, L. (2024). Interface failure of segmental tunnel lining strengthened with steel plates based on fracture mechanics. Frontiers of Structural and Civil Engineering, 18(1), 137–149. doi:10.1007/s11709-024-1019-9.

[7] Yu, T., Zhang, Y., Yan, Z., Zhu, H., & Cao, K. (2025). Methods for determining multiple hazards and response analysis of metro shield tunnels considering existing structural damage. Tunnelling and Underground Space Technology, 162, 106662. doi:10.1016/j.tust.2025.106662.

[8] Huang, W. M., Wang, J. C., Yang, Z. X., & Xu, R. Q. (2022). Analytical method for structural analysis of segmental lining interaction with nonlinear surrounding soil and its application in physical test interpretation. Tunnelling and Underground Space Technology, 127, 104601. doi:10.1016/j.tust.2022.104601.

[9] Huang, W., Zang, Y., Wang, J., Liu, C., Yang, Z., Xu, R., & Fang, H. (2025). General Solution for Longitudinal Response of Shield Tunnel Considering the Effects of Joints and Soil Shear Resistance. International Journal for Numerical and Analytical Methods in Geomechanics, 49(3), 948–960. doi:10.1002/nag.3909.

[10] Liu, Z. X., Ye, X. W., Song, K., Lu, C. R., Song, Y. J., Li, X. J., & Zhao, L. A. (2025). Monitoring-based analysis of the responses of upper structure and tunnel lining during shield tunneling with pile cutting. Tunnelling and Underground Space Technology, 158, 106427. doi:10.1016/j.tust.2025.106427.

[11] Gao, B. Y., Chen, R. P., Wu, H. N., Zhang, Y., & Meng, F. Y. (2024). Full-scale test on the mechanical behavior of longitudinal joints of NC-UHPC composite segments under compression-bending load. Tunnelling and Underground Space Technology, 153, 105993. doi:10.1016/j.tust.2024.105993.

[12] Guo, W., Feng, K., Mu, H., Li, J., Zhou, Y., & He, C. (2025). Investigation on the force transmission performance between segmental rings of super-large cross-section shield tunnels. Tunnelling and Underground Space Technology, 164, 106779. doi:10.1016/j.tust.2025.106779.

[13] Yang, S. Q., Wu, H. N., Cheng, H. Z., Feng, D. L., & Chen, R. P. (2025). A full-ring mechanical model of shield tunnels considering detailed joint configurations. Tunnelling and Underground Space Technology, 164, 106808. doi:10.1016/j.tust.2025.106808.

[14] Zhang, L., He, C., Feng, K., Guo, W. Q., Zhang, J. X., & Xiao, M. Q. (2022). Influence of Bolts on the Compression-bending Capacity of Segmental Joints of Shield Tunnels. Zhongguo Gonglu Xuebao/China Journal of Highway and Transport, 35(11), 195–203. doi:10.19721/j.cnki.1001-7372.2022.11.018.

[15] Zhang, L., Feng, K., He, C., & Xiao, M. (2021). Experimental study on failure behaviors and damage characteristics of segmental joints of shield tunnels. Tumu Gongcheng Xuebao/China Civil Engineering Journal, 54(5), 98–107.

[16] Cao, S. Y., Feng, K., Liu, X., Xiao, M. Q., & He, C. (2021). Experimental Investigation of the Shear Mechanism on Mortise and Tenon Segment Lining. Zhongguo Gonglu Xuebao/China Journal of Highway and Transport, 34(9), 273–284. doi:10.19721/j.cnki.1001-7372.2021.09.023.

[17] Zheng, G., Sun, J., Zhang, T., Zhang, X., Cheng, H., Wang, H., & Diao, Y. (2023). Mechanism and countermeasures of progressive failure in shield tunnels. Tunnelling and Underground Space Technology, 131, 104797. doi:10.1016/j.tust.2022.104797.

[18] Liu, X., Feng, K., Xiao, M. Q., He, C., & Li, C. (2022). Prototype test of a new type segment structure with distributed mortises and tenons for shield tunnel. Gongcheng Lixue/Engineering Mechanics, 39(1), 197–208. doi:10.6052/j.issn.1000-4750.2020.12.0913.

[19] Zhang, D. M., Liu, J., Li, B. J., & Zhong, Y. (2020). Shearing Behavior of Circumferential Joints with Oblique Bolts in Large Diameter Shield Tunnel. Zhongguo Gonglu Xuebao/China Journal of Highway and Transport, 33(12), 142–153. doi:10.19721/j.cnki.1001-7372.2020.12.011.

[20] Shi, C., Wang, Z., Liu, J., Lei, M., Peng, L., & Peng, Z. (2022). Study on ultimate bearing capacity of shield tunnel based on damage model of concrete. Zhongnan Daxue Xuebao (Ziran Kexue Ban)/Journal of Central South University (Science and Technology), 53(11), 4310–4325. doi:10.11817/j.issn.1672-7207.2022.11.012.

[21] Zhang, Y., Liu, T., Zhu, C., & Xiao, J. (2023). Model tests on deformation and failure characteristics of shield tunnel in soil-rock composite stratum under surface surcharge. Journal of Railway Science and Engineering, 20(11), 4277–4287. doi:10.19713/j.cnki.43-1423/u.T20222174.

[22] Ruan, H. F., Liang, R. Z., Kang, C., Li, Z. C., & Ke, Z. B. (2023). Three-dimensional elaborate numerical modelling analysis on the deformation mechanism of metro shield tunnel induced by sudden surface surcharge. Safety and Environmental Engineering, 30(1), 35–45. doi:10.13578/j.cnki.issn.1671-1556.20220162.

[23] Zhu, M., Chen, X., Xia, C., Wang, C., & Bao, X. (2024). Resilience evolution of shield tunnel structures underground surcharge. Yantu Gongcheng Xuebao/Chinese Journal of Geotechnical Engineering , 46(1), 35–44. doi:10.11779/CJGE20221258.

[24] Xie, J., Wang, J., & Huang, W. (2021). Nonlinear structural analysis on cracking behavior of shield tunnel segment under surface loading. Journal of Railway Science and Engineering, 18(1), 162–171. doi:10.19713/j.cnki.43-1423/u.T20200275.

[25] Wang, F. Y., Zhou, M. L., Zhang, D. M., Huang, H. W., & Chapman, D. (2019). Random evolution of multiple cracks and associated mechanical behaviors of segmental tunnel linings using a multiscale modeling method. Tunnelling and Underground Space Technology, 90, 220–230. doi:10.1016/j.tust.2019.05.008.

[26] Yu, H. T., Wu, Y. X., Tu, X. Bin, Zhang, X. Y., & Li, F. (2020). Multi-scale Method for Longitudinal Seismic Response Analysis of Shield Tunnels. Zhongguo Gonglu Xuebao/China Journal of Highway and Transport, 33(1), 138–144. doi:10.19721/j.cnki.1001-7372.2020.01.014.

[27] Liu, J., Shi, C., Gong, C., Lei, M., Wang, Z., Peng, Z., & Cao, C. (2022). Investigation of ultimate bearing capacity of shield tunnel based on concrete damage model. Tunnelling and Underground Space Technology, 125, 104510. doi:10.1016/j.tust.2022.104510.

[28] Sui, Y., Cheng, X., & Zhao, Z. (2023). Research on cracking failure process of concrete components using total strain crack constitutive model. Jianzhu Jiegou Xuebao/Journal of Building Structures, 44(7), 216–224. doi:10.14006/j.jzjgxb.2022.0020.

[29] Fib (International Federation for Structural Concrete). (2013). fib Model Code for Concrete Structures 2010. Ernst & Sohn, Berlin, Germany.

[30] Yu, Y., Wang, J., & Cheng, C. (2025). Fracture and resilience evolution of double-layer lining structure of shield tunnel. Engineering Computations (Swansea, Wales), 42(5), 1771–1790. doi:10.1108/EC-12-2024-1068.

[31] Sun, L. W. (2016). Shield tunnel structure behavior under external load. PhD Thesis, Zhejiang University, Hangzhou, China.

[32] He, C., Liu, C. K., Wang, S. M., Zhang, J. B., Lu, D. Y., & Ma, G. Y. (2018). Influence of Crack Number on Mechanical Properties of Shield Tunnel Segment Structure. Zhongguo Gonglu Xuebao/China Journal of Highway and Transport, 31(10), 210–219.

[33] China GB50011. (2010). Standard for Urban Rail Transit Project Construction. Ministry of Housing and Urban-Rural Development of the People's Republic of Chin, Beijing, China.